Proceedings of ASME Turbo Expo 2009: Power for Land, Sea and Air
GT2009
June 8-12, 2009, Orlando, Florida, USA

GT2009-60026

FLAME TRANSFER FUNCTION MEASUREMENT AND INSTABILITY FREQUENCY PREDICTION USING A THERMOACOUSTIC MODEL

Kyu Tae Kim, Hyung Ju Lee, Jong Guen Lee, Bryan D. Quay, and Domenic Santavicca
Department of Mechanical and Nuclear Engineering,
The Pennsylvania State University, University Park, PA, 16802

ABSTRACT

The dynamic response of a turbulent premixed flame to an acoustic velocity perturbation was experimentally determined in a lean-premixed, swirl-stabilized, lab-scale gas turbine combustor. Fuel was injected far upstream of a choked inlet to eliminate equivalence ratio oscillations. A siren-type modulation device was used to provide acoustic perturbations at the forcing frequency of 100 ~ 400 Hz. To measure global heat release rate, OH*, CH*, and CO_2* chemiluminescence emissions were used. The two-microphone method was utilized to estimate inlet velocity fluctuations, and it was calibrated by direct measurements using a hot wire anemometer under cold-flow conditions. Gain of the flame transfer function (FTF) shows a low pass filter behavior, and it is well-fitted by a second-order model. Phase difference increases quasi-linearly with the forcing frequency. Using the n-τ formulation, gain and phase of FTF were incorporated into an analytic thermoacoustic model in order to predict instability frequencies and corresponding modal structures. Self-excited flame response measurements were also performed to verify eigenfrequencies predicted by the thermoacoustic model. Instability frequency predicted by the thermoacoustic model is supported by experimental results. Two instability frequency bands were measured in the investigated gas turbine combustor at all operating conditions: f ~ 220 Hz and f ~ 350 Hz. Results show that the self-excited instability frequency of f ~ 220 Hz results from the fact that the flames amplify flow perturbations with f = 150 ~ 250 Hz. This frequency range was observed in the flame transfer function measurements. The other instability frequency of f ~ 350 Hz occurs because the whole combustion system has an eigenfrequency corresponding to the ¼-wave eigenmode of the mixing section. This was analytically and experimentally demonstrated. Results also show that the flame length, L_{CH^*max}, plays a critical role in determining self-induced instability frequency.

NOMENCLAUTURE

A	complex amplitude of pressure waves
c	speed of sound
D	diameter
f	forcing frequency
FTF, F	flame transfer function
FWHM	full width at half maximum
HWA	hot wire anemometer
i	$\sqrt{-1}$
k	wave number
K	constant
l, L	length of ducts
n	gain of flame transfer function
P	pressure
PMT	photomultiplier tube
PT	pressure transducer
Q, q	heat release
r	coordinate in radial direction
R	reflection coefficient
S	cross-sectional area
TMM	two-microphone method
V, u	velocity
V	volume
t	time
T	period, temperature
x	coordinate in axial direction
X	mole fraction

GREEK LETTERS

τ	time delay
Φ	equivalence ratio
φ	phase difference
ρ	density
γ	specific heat ratio
ω	angular frequency

Γ_1 section parameter
Γ_2 constant
ξ damping coefficient
Δ difference
λ wavelength

OVERSCRIPTS

$\hat{}$ fluctuation amplitude
$\bar{}$ mean quantity
$\cdot$ time rate of change

SUPERSCRIPTS

+, - down- and upward propagating
` perturbation quantity

SUBSCRIPTS

1 ,2 duct indices
0 ambient quantity
c, comb combustor section
in inlet
max maximum
mean mean value
T total

INTRODUCTION

In order to meet strict emission regulations, lean-premixed, pre-vaporized technology has been adopted for many industrial applications because it reduces the maximum flame temperature, leading to significant reduction of thermal NO_x. Unfortunately, lean premixed flames are susceptible to combustion instability. In general, combustion instability refers to the periodic, high-amplitude pressure fluctuations in a combustion chamber due to the resonant coupling between the system acoustics and the unsteady heat release. Combustion instability is, by nature, related to the energy conversion of thermal to acoustic energy, leading to a self-excited feedback loop. These high amplitude pressure oscillations can substantially reduce performance of a system, and can also destroy part of engines. A large number of experimental, theoretical, and numerical studies have been performed to identify and understand underlying instability driving mechanisms, and also to predict and control the occurrence of instabilities [1-3]. However it is still difficult to accurately predict instability characteristics, i.e., instability frequency and limit-cycle oscillation amplitude, at the development stage. The response of flames to flow perturbations caused by the pressure waves in a combustor is critical information in the theoretical description of combustion-induced oscillations.

For a perfectly premixed flame, the response of a flame can be determined by means of the flame transfer function, where the input function is inlet velocity fluctuation and the output function is heat release rate oscillation. In general, the flame transfer function is expressed by the ratio of the fluctuating components of output to the input functions,

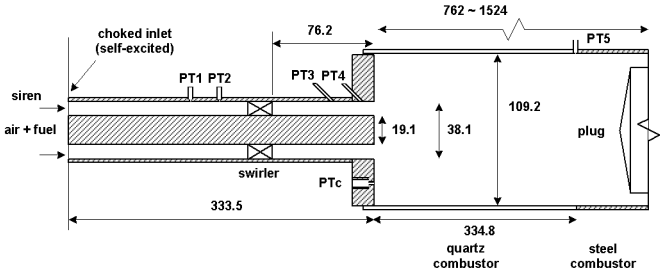

Figure 1. Schematic of a swirl-stabilized, lean-premixed, gas turbine combustor. Dimensions in millimeters.

normalized by their corresponding time-averaged values:

$$FTF(f) = \frac{\dot{Q}'(f)/\bar{\dot{Q}}}{V'(f)/\bar{V}} \tag{1}$$

The flame transfer function can be obtained by experimental methods [4-7], theoretical approaches [8-10], and unsteady CFD calculations [11-13]. Experimental determination of forced flame response is reliable, and it is also required to validate FTF derived theoretically and numerically.

Experimental investigations of the response of a turbulent flame to inlet velocity oscillations and/or equivalence ratio fluctuations have confirmed the underlying mechanisms for nonlinear response and the dynamics of forced flames with respect to changes in inlet operating conditions [4-7]. Applications of FTF measurements to prediction of eigenfrequencies and modal structures of self-excited instabilities have been explored [14, 15]. If the FTF were available, then reduced-order flame response models could be used to predict the onset of instabilities [16, 17]. The FTF can also be used in thermoacoustic network modeling, where the FTF provides a source term, i.e., unsteady heat release in a combustion chamber. Poinsot & Veynante [18] described a general method for one-dimensional thermoacoustic modeling to predict eigenfrequency and corresponding eigenmode.

In this paper, a methodology to predict self-induced instability frequency in a lean premixed gas turbine combustor is described. Flame transfer functions of a turbulent premixed flame are experimentally determined. The gain and phase of the FTF are mathematically formulated by using n-τ model, and they are incorporated into a theoretical thermoacoustic model to predict eigenfrequencies and modal structures. Predicted eigenfrequencies are validated by self-excited flame response measurements. Analytic thermoacoustic modeling and experimental determination of FTF are utilized to interpret self-induced instability observed in a lean-premixed, gas turbine combustor.

Table 1. Test conditions for forced flame response measurements.

parameters	forced response tests
pressure, P	1 atm
inlet temperature, T_{in}	200 °C
nozzle velocity, V_{mean}	60, 70, 80, 90, 100 m/s
overall equivalence ratio, Φ	0.55, 0.60, 0.65, 0.70
forcing frequency, f	100 ~ 400 Hz, Δf = 25 Hz
forcing amplitude, V'/V_{mean}	up to 0.50
fuel composition, X_{H2}	0.00, 0.15, 0.30, 0.45, 0.60

EXPERIMENTAL METHODS

Figure 1 shows a schematic of a lean-premixed, variable-length, gas turbine combustor facility, used in these experiments. This facility consists of an air inlet section, a siren, a mixing section, an optically-accessible quartz combustor section, a steel combustor section, and an exhaust section. A siren-type modulation device is used to provide acoustic modulations. The siren is driven by a variable-speed DC motor, thus providing capabilities for changing forcing frequency (100 ~ 400 Hz). The inlet velocity fluctuation amplitudes (V'/V_{mean}) can be varied by controlling the relative amount of air/fuel flow through the modulating device. At the entrance to the mixing section the flow is choked. This provides a well-defined acoustic boundary condition for self-excited flame response measurements. For forced flame response measurements, the choking plate is removed and mounted upstream of the siren. The fuel is injected and mixed far upstream of the choked inlet to create spatially and temporally homogeneous reactant mixtures before they enter a reaction zone.

The combustor consists of a stainless steel dump plane, to which an optically accessible fused-silica combustor with a 109.2 mm-diameter and 334.8 mm-length is attached. The downstream end of the quartz combustor is connected to a stainless steel variable-length combustor section. The length of the combustor can be continuously varied between 762 mm (30 inch) and 1524 mm (60 inch) by moving a water-cooled plug along the length of the steel combustor section. The overall combustor length is defined as the distance from the combustor dump plane to the plug. Detailed dimensions are included in Fig. 1.

PCB 112A04 piezoelectric transducers with charge amplifiers are used to measure unsteady pressure perturbations in the mixing and the combustor sections. Two pressure transducers located at 12.7 mm and 50.8 mm upstream of the combustor dump plane are used to estimate the inlet velocity fluctuations using the two-microphone method [19, 20]. To calibrate the two-microphone method, direct measurements of velocity fluctuations are performed under cold flow conditions with a TSI 1210-20 constant temperature hot-wire anemometer. Three photomultiplier tubes (PMT, Hamamatsu

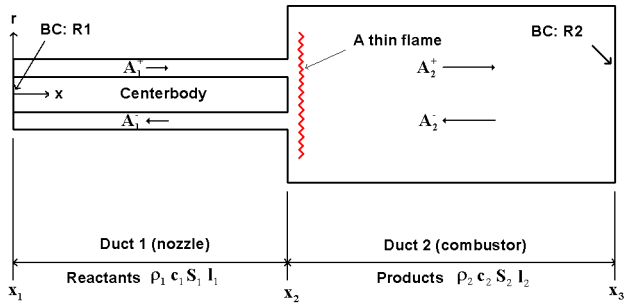

Figure 2. Decomposition of the combustor into three acoustic sub-elements.

model H7732-10) are used to measure the global OH* (307 ± 5 nm), CH* (432 ± 5 nm), and CO_2* (365 ± 5 nm) chemiluminescence emission intensities from a whole flame. Quantitative description of the flame's heat release perturbations is based on the experimental observation that for a fixed equivalence ratio, the intensity of chemiluminescence emission increases linearly with the fuel flow rate [1-2]. But this observation was made under stable flow conditions. The assumption that OH*, CH*, or CO_2* chemiluminescence emissions from a whole flame can be used as a quantitative indicator of the flame's heat release rate oscillations should be proved under unsteady flow conditions as well. The quantification of chemiluminescence measurements is an important issue [21-23]. This is, however, beyond the scope of the present contribution. The issue is left for future studies. An ICCD camera (Princeton Instruments model 576G) with a CH* band pass filter centered at 430 nm (10 nm FWHM) is used to record the flame images. The field of view of the photomultipliers and the ICCD camera is such that they cover the entire combustion zone, and it is ensured that three PMTs view the same region. A three-point Abel deconvolution procedure is used to reconstruct the two-dimensional structure of the flame from the line-of-sight integrated CH* chemiluminescence images.

All tests were performed at a mean pressure of 1 atm and at mean equivalence ratios ranging from 0.55 to 0.70. For the present study, forcing frequencies were varied from 100 to 400 Hz, which includes self-sustained instability frequencies observed in the rig, shown in Fig. 1. To reduce the influence of the system's acoustics on upstream forcing, the combustor length was kept the shortest, 0.584 m. At this condition, resonance frequency of the system is much higher than the forcing frequency and therefore the resonant effects are minimized. The fuel was pure natural gas or a mixture of natural gas and H_2 by volume. The H_2 percentage content in the fuel mixture is referred to the total volumetric fuel flow rate:

$$\%H_2 = \frac{\dot{V}_{H_2}}{\dot{V}_{H_2} + \dot{V}_{N.G.}} \quad (2)$$

The full list of operating conditions and fuel compositions for forced flame response measurements is listed in Table 1.

Experimental data were obtained with a National Instrument data acquisition system controlled by Labview software. 16,384 data points were taken at a sampling rate of 8192 Hz, which resulted in a frequency resolution of 0.5 Hz and a time resolution of 0.122 msec. Spectral analysis of the signals was performed using the fast Fourier transform (FFT) technique.

LINEAR STABILITY ANALYSIS

Thermoacoustic systems can be modeled efficiently as networks of acoustic elements, where each element corresponds to a certain component of the system [24]. Figure 2 shows a combustion system modeled as an ensemble of acoustic sub-elements. The whole combustor can be decomposed into acoustic sub-elements such as the mixing section, the swirler, the flame, and the combustor. However, in this model the swirler is not taken into account inasmuch as its influence on the acoustic field in the mixing section is negligible. This is because acoustic pressure measurements up- and downstream of the swirler using PT1 through PT4 shown in Fig. 1 confirmed that amplitude and phase of pressure waves are not significantly affected by the existence of the swirler; the swirler is acoustically transparent.

The ratio of the transverse dimensions to the acoustic wavelength is very small (D/λ ~ 0.0332), and therefore we assume that only longitudinal eigenmodes are developed. It is also assumed that the flame sheet is infinitesimally thin, because the flame length is much smaller than the acoustic wavelength. In practice, combustion occurs over a distributed region of heat release [25]. If the reaction zone is not compact, locally defined FTF gain and phase should be used [26]. The combustor exit is partially restricted by a plug, and the blockage ratio is approximately 80% (see Fig. 1). This situation may give some uncertainty in the predicted eigenfrequencies because entropy waves may induce upward propagating pressure perturbations [27]. In a previous work, a burner with an open end was used by Noiray et al. [28] to avoid this uncertainty.

According to linear acoustic theory, governing equations for acoustic velocity and pressure in low-speed reacting flows can be expressed in the following equations [18, 29]:

$$\frac{\partial u'}{\partial t} + \frac{1}{\rho_0}\frac{\partial p'}{\partial x} = 0 \quad (3)$$

$$\frac{1}{\gamma p_0}\frac{\partial p'}{\partial t} + \frac{1}{S}\frac{\partial (Su')}{\partial x} = \frac{\gamma - 1}{\gamma p_0} q_T' \quad (4)$$

where $\rho_0 = \rho_0(x)$ is the mean density; $S = S(x)$ is the cross-sectional area; γ is the specific heat ratio; q_T' is the unsteady heat release rate [W/m^3]. Integrating Equations (3) and (4) from x_2^- to x_2^+ and taking the limit where x_2^- and x_2^+ go to x_2, acoustic jump conditions for a thin flame can be obtained.

$$p'(x_2^+) = p'(x_2^-) \quad (5)$$

$$S(x_2^+)u'(x_2^+) - S(x_2^-)u'(x_2^-) = \frac{\gamma - 1}{\gamma p_0}\dot{Q}_T' \quad (6)$$

Assuming harmonic variation of any acoustic variable, the acoustic pressure and velocity in duct 1 and 2 may be expressed in the following forms:

$$p_1' = \hat{p}_1 e^{-i\omega t} = A_1^+ e^{ik_1(x-x_1)-i\omega t} + A_1^- e^{-ik_1(x-x_1)-i\omega t} \quad (7)$$

$$u_1' = \hat{u}_1 e^{-i\omega t} = \frac{A_1^+}{\rho_1 c_1} e^{ik_1(x-x_1)-i\omega t} - \frac{A_1^-}{\rho_1 c_1} e^{-ik_1(x-x_1)-i\omega t} \quad (8)$$

$$p_2' = \hat{p}_2 e^{-i\omega t} = A_2^+ e^{ik_2(x-x_2)-i\omega t} + A_2^- e^{-ik_2(x-x_2)-i\omega t} \quad (9)$$

$$u_2' = \hat{u}_2 e^{-i\omega t} = \frac{A_2^+}{\rho_2 c_2} e^{ik_2(x-x_2)-i\omega t} - \frac{A_2^-}{\rho_2 c_2} e^{-ik_2(x-x_2)-i\omega t} \quad (10)$$

Substituting Equations (7) - (10) into Equations (5) and (6), and assuming harmonic time dependence of the unsteady heat release, $\dot{Q}_T' = \hat{Q} e^{-i\omega t}$,

$$A_2^+ + A_2^- = A_1^+ e^{ik_1 l_1} + A_1^- e^{-ik_1 l_1} \quad (11)$$

$$\frac{S_2}{\rho_2 c_2}(A_2^+ - A_2^-) = \frac{S_1}{\rho_1 c_1}(A_1^+ e^{ik_1 l_1} - A_1^- e^{-ik_1 l_1}) + \frac{\gamma - 1}{\gamma p_0}\hat{Q} \quad (12)$$

Let's define a section parameter, which represents the ratio of the acoustic impedances at the interface of duct 1 and 2.

$$\Gamma_1 = \frac{\rho_2 c_2 S_1}{\rho_1 c_1 S_2} \quad (13)$$

Rearranging Equation (11) and (12) using (13) as a matrix form, we can get the following equation:

$$\begin{pmatrix} A_2^+ \\ A_2^- \end{pmatrix} = \frac{1}{2}\begin{bmatrix} e^{ik_1 l_1}(1+\Gamma_1) & e^{-ik_1 l_1}(1-\Gamma_1) \\ e^{ik_1 l_1}(1-\Gamma_1) & e^{-ik_1 l_1}(1+\Gamma_1) \end{bmatrix}\begin{pmatrix} A_1^+ \\ A_1^- \end{pmatrix} + \frac{1}{2}\frac{\rho_2 c_2}{S_2}\frac{\gamma - 1}{\rho_1 c_1^2}\begin{pmatrix} \hat{Q} \\ -\hat{Q} \end{pmatrix} \quad (14)$$

Let's consider the boundary conditions. From Equation (7) to (10),

$$\frac{A_1^+}{A_1^-} = R_1 \tag{15}$$

$$\frac{A_2^+}{A_2^-} e^{2ik_2 l_2} = R_2 \tag{16}$$

R_1 and R_2 denote the reflection coefficients at the inlet and outlet boundaries. Equation (14) and its BC's (15) and (16) lead to a linear system which has a non-trivial solution only for a limited set of angular frequency. To close the system, however, the unsteady heat release, $\hat{Q}$, should be provided. It can be obtained from analytic, experimental, and numerical simulation methods. Here, flame transfer function measurements are used by means of the classical n-τ model. The flame transfer function is defined as

$$F(\omega) = \frac{\hat{Q}/\bar{Q}}{\hat{u}/\bar{u}} \tag{17}$$

The flame transfer function is cast in the following form:

$$F(\omega) = \frac{\hat{Q}/\bar{Q}}{\hat{u}/\bar{u}} = n(\omega) e^{i\omega\tau} \tag{18}$$

Gain and phase are modeled separately. Gain can be modeled as a second order function to represent the overshoot behavior as can be seen later, and phase typically linearly increases with frequency.

$$\Delta\varphi = \omega\tau \tag{19}$$

$$n(\omega) = \left| \frac{K}{1 + i2\xi(\omega/\omega_c) - (\omega/\omega_c)^2} \right| \tag{20}$$

The constants τ, ξ, K, and ω_c are determined from empirical fits of Equations (19) and (20). Substituting Equation (18) into Equation (14) and after some manipulation, we get the dispersion relation:

$$\frac{1}{R_2}\left(1 + \Gamma_1 + \Gamma_2 n e^{i\omega\tau}\right) + \frac{1}{R_1 R_2} e^{-2ik_1 l_1}\left(1 - \Gamma_1 - \Gamma_2 n e^{i\omega\tau}\right)$$
$$- e^{-2ik_2 k_2}\left(1 - \Gamma_1 - \Gamma_2 n e^{i\omega\tau}\right) - \frac{1}{R_1} e^{-2i(k_1 l_1 + k_2 l_2)}\left(1 + \Gamma_1 + \Gamma_2 n e^{i\omega\tau}\right) = 0 \tag{21}$$

where, $\Gamma_2 = \frac{\rho_2 c_2}{\rho_1 c_1 S_2} \frac{\gamma - 1}{\rho_1 c_1^2} \frac{\bar{Q}}{\bar{u}}$

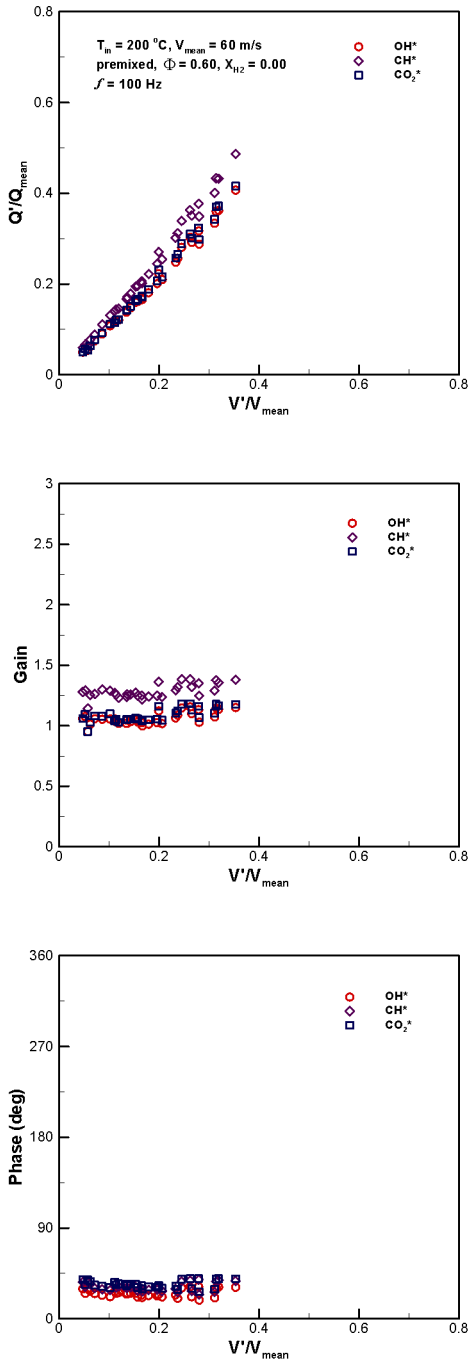

Figure 3. Normalized heat release response, the gain and phase difference of flame transfer function vs. forcing amplitude. Operating conditions: T_{in} = 200 °C, V_{mean} = 60 m/s, Φ = 0.60, X_{H2} = 0.00, and *f* = 100 Hz.

Equation (21) determines the eigenfrequencies of the system by solving for the real and imaginary parts of the angular frequency, ω. If the imaginary part of ω is positive, the

solution is unstable and combustion instability is expected. The instability frequency is obtained from the real part of ω. This linear stability analysis can be extended to capture nonlinear features of self-sustained instability using nonlinear flame transfer functions.

RESULTS AND DISCUSSION

Flame Transfer Function Measurements

Figure 3 shows the amplitude dependence of the normalized heat release response, the gain, and phase difference of FTF at a modulation frequency of f = 100 Hz (T_{in} = 200 °C, V_{mean} = 60 m/s, Φ = 0.60, X_{H2} = 0.00). Measurements of OH*, CH*, and CO_2* chemiluminescence emission intensities are used as an indicator of heat release rate oscillations. The normalized heat release response and the gain of CH* chemiluminescence are a little higher than those of OH* and CO_2* chemiluminescence, but they show similar behavior. For any levels of inlet velocity modulation, the coherence between inlet velocity and chemiluminescence signals at the forcing frequency was close to unity, enabling flame transfer functions to be accurately measured. It can be observed that the normalized heat release response linearly increases with the forcing amplitude, up to $V'/V_{mean} \sim 0.360$. The maximum driving amplitude point is not caused by flame blowoff, but by a limitation of the modulating device. The gain (nondimensional, see Eq. 1) is virtually constant with respect to the forcing amplitude, representing the flame response is linear. The flame length is stretched or contracted without shear layer rollup. The phase difference of the flame transfer function is nearly independent of the forcing amplitude, implying that the center of heat-release (maximum heat release location) is not affected by forcing amplitude. However, as shown in Fig. 4, the flame transfer function measurements at the forcing frequency of f = 200 Hz clearly show the nonlinear flame response. At the forcing amplitude of $V'/V_{mean} \sim 0.10$ where the flame response was linear for the modulation at 100 Hz, the gain of FTF drops abruptly with increases in the forcing amplitude, and the gain gradually decreases to a certain value, i.e., 1.5.

It is known that this saturation phenomenon is related to a nonlinear evolution of the flame surface area [4-6]. In particular, the minimum level of the inception of the nonlinear flame response decreases with increasing modulation frequency [6, 30]. With increases in the forcing amplitude, the phase difference of FTF is constant for $V'/V_{mean} > 0.10$, irrespective of the nonlinear behavior of the gain. Several factors affect nonlinear flame dynamics: unsteady flame liftoff [31, 32], local/global extinction [31, 33], equivalence ratio oscillation [34], and shear layer rollup [4, 5, 30]. Amplitude-dependent phase behavior and drastic change in the gain of FTF weren't observed in the combustor at any operating conditions investigated, implying that the evolution of flame surface area is influenced by the shear layer rollup and the turbulent motion of the flame. Because OH*, CH*, and CO_2* chemiluminescence shows similar behavior in terms of the gain and phase difference of FTF at all operating conditions, only CH* results will be presented in the remainder of this

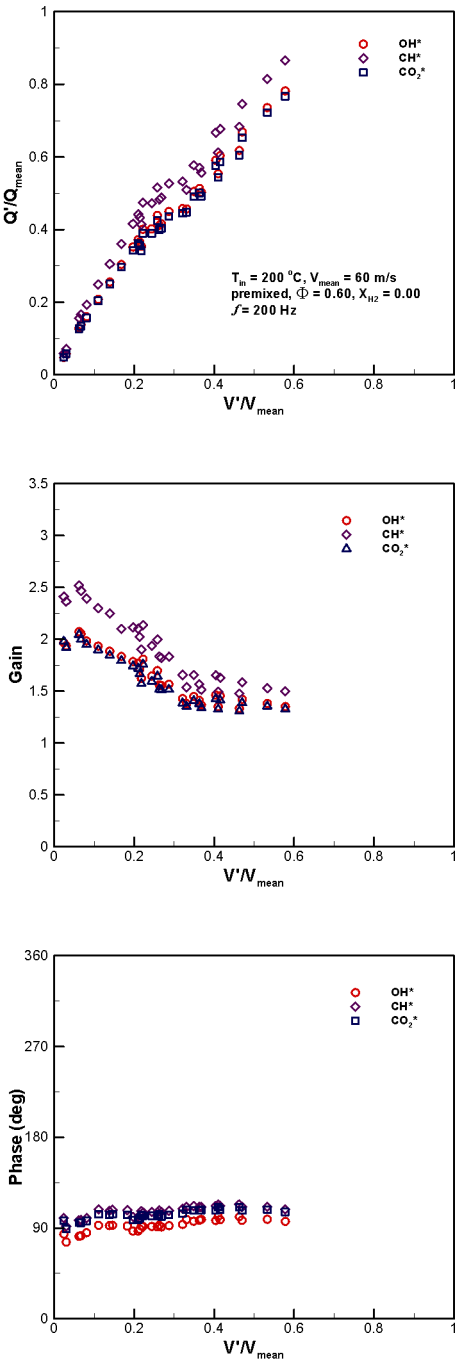

Figure 4. Normalized heat release response, the gain and phase difference of flame transfer function vs. forcing amplitude. Operating conditions: T_{in} = 200 °C, V_{mean} = 60 m/s, Φ = 0.60, X_{H2} = 0.00, and f = 200 Hz.

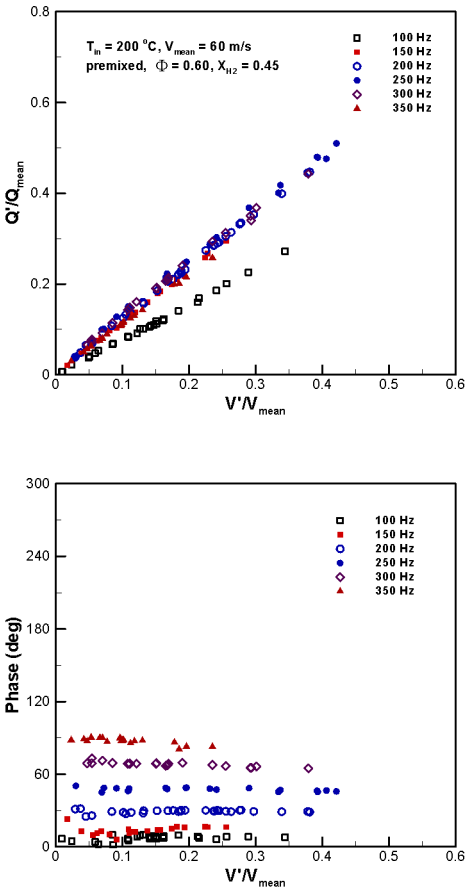

Figure 5. Normalized heat release response and phase difference of flame transfer function vs. forcing amplitude. Operating conditions: T_{in} = 200 °C, V_{mean} = 60 m/s, Φ = 0.60, X_{H2} = 0.45, f = 100, 150, 200, 250, 300, 350 Hz.

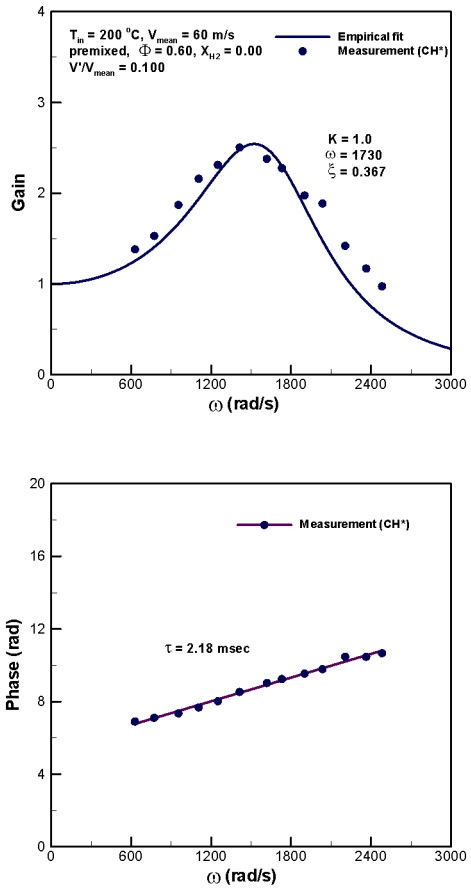

Figure 6. Gain and phase difference of FTF and their corresponding theoretical fits. Operating conditions: T_{in} = 200 °C, V_{mean} = 60 m/s, Φ = 0.60, X_{H2} = 0.00, and V'/V_{mean} = 0.100.

paper.

Figure 5 shows a typical example of the heat release response of flames with high H_2 mole fraction (T_{in} = 200 °C, V_{mean} = 60 m/s, Φ = 0.60, X_{H2} = 0.45). As the fraction of H_2 increases, the flame shape changes from "V-shaped" to "M-shaped" and the flame length decreases most likely due to the increase of flame speed [35]. Different from the cases without H_2-enrichment but at the same inlet flow condition, the flame tends to remain in the linear regime even at high forcing frequency (f = 350 Hz) and amplitude (V'/V_{mean} = 0.235). The phase difference increases with forcing frequency, and it is independent of forcing amplitude. Similar observations have been made from experimental and theoretical investigations of laminar premixed flames [36, 37]. It was observed that the "V" flame's gain is greater than the "M" flame's gain for a given frequency, because "M" flames produce weak flame surface fluctuations when they interact with flow disturbances [35]. It is then suggested that the "M" flames may not be susceptible to combustion dynamics, as compared to the "V" flames. As will be discussed in the last section, the modification of the steady-state flame shape from "V" to "M" flames by H_2-enrichment indeed reduces the limit-cycle pressure oscillation amplitude. Phase-resolved flame imaging is necessary to elucidate the linear/nonlinear responses of an enveloped "M" flame. This study is in progress.

n-τ Formulation

Figure 6 presents the gain and phase difference of FTF at a constant forcing amplitude, V'/V_{mean} = 0.100 (Operating conditions: T_{in} = 200 °C, V_{mean} = 60 m/s, Φ = 0.60, premixed, X_{H2} = 0.00). The flame response at this level of modulation remains in the linear regime. With increasing the modulation frequency, the gain increases and reaches its maximum value at f = 225 Hz. Then, the gain gradually

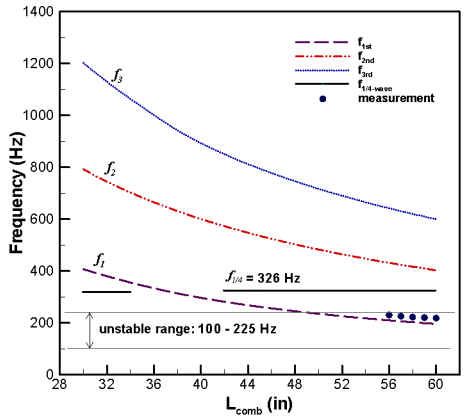

Figure 7. Eigenfrequencies calculated by thermoacoustic model and self-excited instability frequencies (measurement) as a function of the combustor length. Operating conditions: T_{in} = 200 °C, V_{mean} = 60 m/s, Φ = 0.60, and X_{H2} = 0.00.

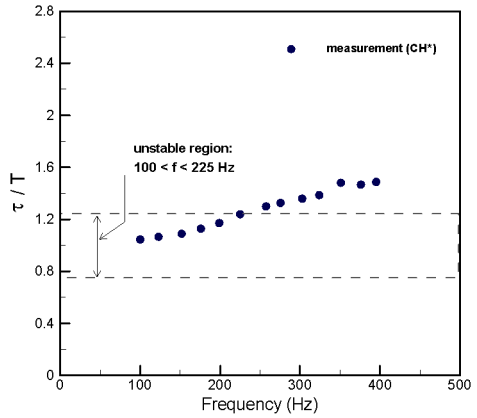

Figure 8. The ratio of convection time to the acoustic period vs. forcing frequency. Operating conditions: T_{in} = 200 °C, V_{mean} = 60 m/s, Φ = 0.60, and X_{H2} = 0.00.

decreases close to zero in the high frequency limit. The gain of FTF exhibits an overshoot which is also observed in other studies [4, 14, 30, 36]. The phase increases quasi-linearly with forcing frequency. Also, the gain and the phase are empirically fitted into the equations (19) and (20) as shown in Fig. 6. From these fitting, the following parameter values are obtained: ξ = 0.367, ω_c = 1730, K = 1.000 and τ = 2.18 msec. These values are found to be strongly dependent on fuel composition [35]. These parameters are substituted into Equation (21) to solve for eigenvalues of the system.

Eigenfrequency Prediction

Mean temperatures in each section were assumed to be constant, and thermodynamic properties of fresh and burnt gases were calculated by the ideal gas law (at inlet or mean combustor temperature). The combustor temperature, T_2 (1120 °C) was assumed to be the adiabatic flame temperature (T_{ad} = 1320 °C). The exit gas temperature was measured by a thermocouple as T_{exit} = 920 °C. The downstream end of the combustor, R_2 = 1, was assumed to be a velocity node point, but the inlet boundary condition, R_1 = 0.212*exp (-i*0.410), was obtained from self-induced flame response measurements. Using the wave decomposition method, the amplitude of up- and downward propagating acoustic pressure waves can be calculated (refer to the schematic in Fig. 2). It was found that the amplitude of upward traveling waves (A_1^-) is greater than that of downward traveling waves (A_1^+) by a factor of 5. Traveling waves exist in the mixing section and the acoustics in the mixing section is driven by high-amplitude pressure oscillations in the combustion chamber. With these boundary conditions, experimentally determined flame transfer functions were incorporated into the thermoacoustic model to solve the dispersion relation. Equation (21) was numerically resolved by varying the combustor length, l_2, which was used as a bifurcation parameter. Figure 7 shows eigenfrequencies calculated by the thermoacoustic model and measurement results (symbols): T_{in} = 200 °C, V_{mean} = 60 m/s, Φ = 0.60, premixed, X_{H2} = 0.00. The three curves, f_1, f_2, and f_3, correspond to the lowest three longitudinal mode eigenfrequencies as a function of the combustor length. The longer the combustor length, the lower the eigenfrequencies. Also, shown as a horizontal line (f = 326 Hz) in the Fig. 7 is the calculated ¼-wave resonant frequency of the mixing section at the given inlet temperature, T_{in} = 200 °C, which is independent of the combustor length. It is interesting to note that the ¼-wave eigenmode does not occur at the combustor length of 35" < L_{comb} < 41", presumably because the ¼-wave eigenmode competes with the first longitudinal mode, f_1, and therefore, only one eigenmode is selected. At this operating condition, the strongest self-excited instability was observed at L_{comb} = 60" (f = 219 Hz and $P_c'/P_{c,\ mean}$ = 0.0534). Eigenfrequencies predicted by the analytic model agree with experimental measurements, and the observed eigenmode corresponds to the first longitudinal mode.

To determine the range of instability frequencies, the time-lag model was used. With a choked inlet, pressure leads velocity by 90° at the combustor dump plane. Therefore, the first unstable regime is determined by 0.75 < τ/T < 1.25. Figure 8 presents the ratio of the convection time to the acoustic period vs. forcing frequency at the same operating condition, showing that unstable frequency range is between 100 Hz and 225 Hz. The convection time delay was calculated from the phase information of FTF. Applying this unstable

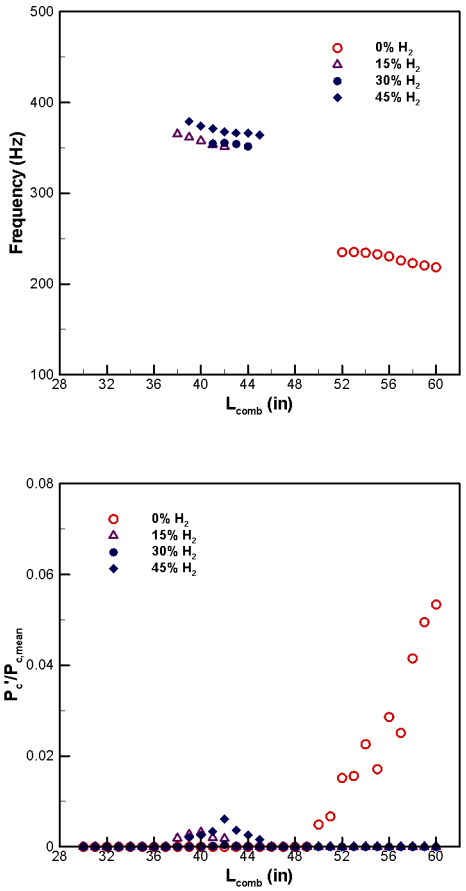

Figure 9. Dependence of self-excited instability frequency and intensity on H_2 mole fraction. Operating conditions: T_{in} = 200 °C, V_{mean} = 60 m/s, Φ = 0.60, and X_{H2} = 0.00, 0.15, 0.30, 0.45.

frequency range to the result of thermoacoustic modeling, as shown in Fig. 7, instability frequency prediction by the thermoacoustic model and the time-lag analysis shows good agreement with measured instability frequency band.

Self-Excited Instability Measurements

To verify thermoacoustic model predictions, self-excited flame response measurements were characterized in a lean-premixed, variable-length, gas turbine combustor facility, shown in Fig. 1. The capability to vary the combustor length enables to control the acoustic eigenfrequencies of the combustion system at a given operating condition. Figure 9 shows the dependence of self-excited instability frequency and intensity ($P_c'/P_{c,\,mean}$) upon H_2 mole fraction: T_{in} = 200 °C, V_{mean} = 60 m/s, Φ = 0.60, X_{H2} = 0.00, 0.15, 0.30, 0.45. At X_{H2} = 0.00, the strongest instability, $P_c'/P_{c,\,mean}$ = 0.0534, is found for the combustor length of L_{comb} = 60" at f = 219 Hz. In contrast, the instability frequencies increase to 368 Hz at X_{H2} =

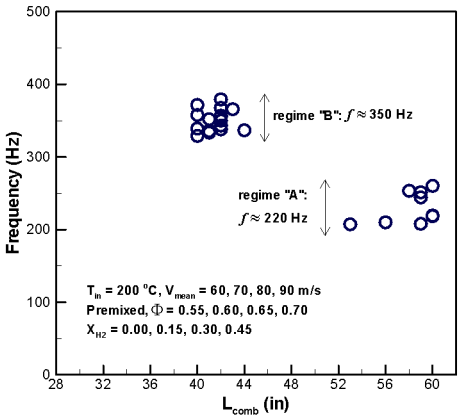

Figure 10. Dependence of self-excited instability frequency upon the combustor length. Note that the cases where the intensity of instability is strongest are presented for each operating condition. Operating conditions: T_{in} = 200 °C, V_{mean} = 60, 70, 80, 90 m/s, Φ = 0.55, 0.60, 0.65, 0.70, and X_{H2} = 0.00, 0.15, 0.30, 0.45.

0.45 and the strongest instability intensity is observed at L_{comb} = 42". The normalized combustor pressure oscillation amplitude decreases by a factor of 9 when the H_2 mole fraction (X_{H2}) changes from = 0.00 to 0.45. The significant reduction in the instability intensity may be associated with changes in the flame structure from "V-shaped" to "M-shaped" flames as X_{H2} increases. This is consistent with forced flame response measurement results in that the forced response of a flame with X_{H2} = 0.45 tends to remain in the linear regime for a relatively high level (up to 24%) of inlet velocity fluctuation at the forcing frequency of 350 Hz, which is close to the self-sustained instability frequency at the same operating condition. The flame transfer function (FTF) measurement results for the same combustor [35] show that the gain of FTF decreases with increasing H_2 mole fraction for a given inlet flow condition and at the same forcing frequency.

Figure 10 shows the dependence of the instability frequency upon the combustor length. The inlet flow conditions are: T_{in} = 200 °C, V_{mean} = 60, 70, 80, 90 m/s, Φ = 0.55, 0.60, 0.65, 0.70, premixed, X_{H2} = 0.00, 0.15, 0.30, 0.45. It should be noted that the cases where the intensity of instability is strongest are presented for each operating condition, even though the instabilities occur over a certain range of combustor length. Two instability frequency bands are observed. Regime "A" corresponds to f ~ 220 Hz at L_{comb} ~ 60", and regime "B" corresponds to f ~ 350 Hz at L_{comb} ~ 41". No instability was observed at L_{comb} < 38" and 45" < L_{comb} < 53".

In order to interpret the reasons why the coupling between the system acoustics and convection of flow perturbations occurs at only f ~ 220 Hz and f ~ 350 Hz, the dependence of self-excited instability frequency upon the

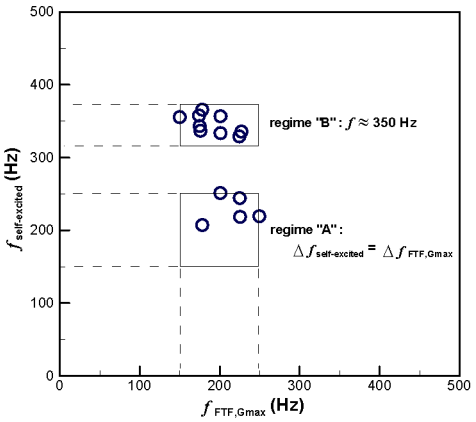

Figure 11. Dependence of self-excited instability frequency upon the modulation frequency, where the gain reaches its maximum value: T_{in} = 200 °C, V_{mean} = 60, 70, 80 m/s, Φ = 0.55, 0.60, 0.65, 0.70, and X_{H2} = 0.00, 0.15, 0.30, 0.45.

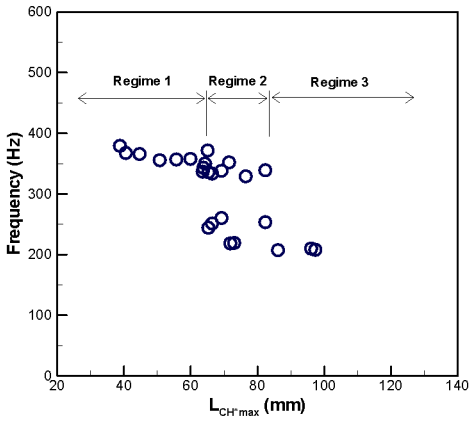

Figure 12. Dependence of self-excited instability frequency upon flame length, L_{CH^*max}. Operating conditions: T_{in} = 200 °C, V_{mean} = 60, 70, 80, 90 m/s, Φ = 0.55, 0.60, 0.65, 0.70, and X_{H2} = 0.00, 0.15, 0.30, 0.45.

modulation frequency, where the gain of FTF reaches its maximum value, is shown in Fig. 11. The regime "A" (the lower box) denotes the self-induced instability frequencies, which is consistent with forcing frequencies. We observed that the modulation frequency in which the flame response is relatively strong is 150 ~ 250 Hz, regardless of operating conditions [35]. This means that the flame has a preferred range of frequency where its response is maximum. Meanwhile, regime "B" (the upper box) corresponds to the ¼-wave eigenfrequency of the mixing section, already shown in Fig. 7. Although standing waves are not developed in the mixing section, the combustion system has the eigenfrequency corresponding to the ¼-wave resonance frequency of the mixing section. Hence, at certain operating conditions, the 1/4-wave eigenmode of the mixing section is excited by the unsteady combustion process, leading to self-sustained pressure oscillations. Similar observation has been reported by Dowling et al. [38]. They reported that an eigenmode of a system was associated with a resonance of the supply plenum. An analytic thermoacoustic model provides infinite number of eigenfrequencies at a given condition, but only selected eigenfrequencies are excited in measurements.

Combustion instability occurs when periodic disturbance convection process couples with acoustic eigenmodes of the combustor. Acoustic eigenfrequencies are determined by speed of sound and the length between the combustor dump plane and the exit of the combustor. However, the convection process is governed by input parameters and the geometry of the nozzle. The distance between the edge of the centerbody and the maximum CH* chemiluminescence intensity location plays a critical role in combustion instability, since the convection time scale is determined by the distance, L_{CH^*max} [30, 39, 40]. Figure 12 plots the dependence of instability frequencies upon flame length, L_{CH^*max}. The instability frequency is divided into three distinct regimes. In regime I, the instability frequency is approximately 350 Hz at L_{CH^*max} < 65 mm, representing flames with short flame length. In regime III, however, the instability frequency of $f \sim 220$ Hz was observed at L_{CH^*max} > 85 mm. In the intermediate range, regime II, both instability frequencies were measured. Flames in regime II can couple with both eigenmodes of the system. This indicates that the flame length is an important parameter playing a role in determining self-excited instability frequencies among infinite number of acoustic eigenfrequencies of a system. Also, the flame length was found to be one of relevant parameters controlling the response of swirl-stabilized, turbulent premixed flames [30, 35]. In the present study, we examined how to predict self-sustained instability frequencies using an analytic model and the relationship between forced flame responses and self-excited responses in order to interpret combustion instability.

CONCLUSIONS

Flame transfer function measurements were taken in a lean-premixed, swirl-stabilized, gas turbine combustor. The forced response of turbulent premixed flames was incorporated into an analytic thermoacoustic model to predict eigenfrequencies of the system. Predictions showed a good agreement with measurement results. Theoretical models improve our understanding of combustion instability in lean premixed combustors. Particularly, it was shown that the instability frequency of $f \sim 220$ Hz observed in self-excited flame response measurements corresponds to the modulation frequency, where gain of FTF is highest. The other instability

frequency of $f \sim 350$ Hz corresponds to the ¼-wave eigenmode frequency of the mixing section. Although the flame response is relatively weak at this frequency, the resonance in the mixing section strengthens the self-excited instability. Also, results show that fuel composition has substantial impacts on flame shape, leading to significant influence upon the forced and self-excited flame responses. The enveloped "M" flames are less susceptible to combustion instability as long as it doesn't couple with high-frequency resonance of a system. With high H_2 mole fraction, self-excited instability frequency increased, and the normalized combustor pressure oscillation amplitude decreased significantly. The detailed measurements discussed in this paper are critical to the formulation and identification of eigenmodes of the combustion system, and to improving our understanding of the influence of fuel composition upon forced and self-excited flame responses.

REFERENCES

[1] Lee, J.G. and Santavicca, D.A., 2003, "Experimental diagnostics for the study of combustion instabilities in lean premixed combustors," J. Propul. Power, **19**, pp. 735-750.

[2] Lieuwen, T. and Yang, V., "Combustion instabilities in gas turbine engines," Progress in Astronautics and Aeronautics, vol. 210, AIAA, Washington, DC, 2005.

[3] Candel, S., 2002, "Combustion dynamics and control: progress and challenges," Proc. Combust. Instit., **29**, pp. 1-28.

[4] Balachandran, R., Ayoola, B.O., Kaminski, C.F., Dowling, A.P., and Mastorakos, E., 2005, "Experimental investigation of the nonlinear response of turbulent premixed flames to imposed inlet velocity oscillations," Combust. Flame, **143**, pp. 37-55.

[5] Bellows, B.D., Neumeier, Y., and Lieuwen, T., 2006, "Forced response of a swirling, premixed flame to flow disturbances," J. Propul. Power, **22**, pp. 1075-1084.

[6] Kulsheimer, C. and Buchner, H., 2002, "Combustion dynamics of turbulent swirling flames," Combust. Flame, **131**, pp. 70-84.

[7] Lieuwen, T. and Neumeier, Y., 2002, "Nonlinear pressure-heat release transfer function measurements in a premixed combustor," Proc. Combust. Instit., **29**, pp. 99-105.

[8] You D., Huang, Y., and Yang, V., 2005, "A generalized model of acoustic response of turbulent premixed flame and its application to gas-turbine combustion instability analysis," Combust. Sci. and Tech., **177**, pp. 1109-1150.

[9] Fleifil, M., Annaswamy, A.M., Ghoneim, Z.A., and Ghoniem, A.F., 1996, "Response of a laminar premixed flame to flow oscillations: a kinematic model and thermoacoustic instability results," Combust. Flame, **106**, pp. 487-510.

[10] Preetham, S.H. and Lieuwen, T., 2007, "Response of turbulent premixed flames to harmonic acoustic forcing," Proc. Combust. Instit., **31**, pp. 1427-1434.

[11] Armitage, C.A., Balachandran, R., Mastorakos, E., and Cant, R.S., 2006, "Investigation of the nonlinear response of turbulent premixed flames to imposed inlet velocity oscillations," Combust. Flame, **146**, pp. 419-436.

[12] Sengissen, A.X., Van Kampen, J.F., Huls, R.A., Stoffels, G.G.M., Kok, J.B.W., and Poinsot, T.J., 2007, "LES and experimental studies of cold and reacting flow in a swirled partially premixed burner with and without fuel modulation," Combust. Flame, **150**, pp. 40-53.

[13] Gentemann, A., Hirsch, C., Kunze, K., Kiesewetter, F., Sattelmayer, T., and Polifke, W., 2004, "Validation of flame transfer function reconstruction for perfectly premixed swirl flames," Proceedings of ASME Turbo Expo 2004, Vienna, Austria, June 14-17.

[14] Noiray, N., Durox, D., Schuller, T., and Candel, S., 2006, "Self-induced instabilities of premixed flames in a multiple injection configuration," Combust. Flame, **145**, pp. 435-446.

[15] Bellucci, V., Schuermans, B., Nowak, D., Flohr, P., and Paschereit, C.O., 2005, "Thermoacoustic modeling of a gas turbine combustor equipped with acoustic dampers," J. Eng. Gas Turb. Power, **127**, pp. 372-379.

[16] Huang, Y. and Baumann, W.T., 2007, "Reduced-order modeling of dynamic heat release for thermoacoustic instability prediction," Combust. Sci. and Tech., **179**, pp. 617-636.

[17] Ananthkrishnan, N., Deo, S., and Culick, F.E.C., 2005, "Reduced-order modeling and dynamics of nonlinear acoustic waves in a combustion chamber," Combust. Sci. and Tech., **177**, pp. 221-247.

[18] Poinsot, T.J. and Veynante, D.P., 2005, "Theoretical and Numerical Combustion," 2nd ed. Edwards, Ann Arbor, MI.

[19] Waser, M.P. and Crocker, M.J., 1984, "Introduction to the two-microphone cross-spectral method of determining sound intensity," Noise Control Eng. J., **22**, pp. 76-85.

[20] Abom, M. and Boden, H., 1988, "Error analysis of two-microphone measurements in ducts with flow," J. Acoust. Soc. Am., **83**, pp. 2429-2438.

[21] Panoutsos, C.S., Hardalupas, Y., and Taylor, A.M.K.P., 2009, "Numerical evaluation of equivalence ratio measurement using OH* and CH* chemiluminescence in premixed and non-premixed methane-air flames," Combust. Flame, **156**, pp. 273-291.

[22] Higgins, B., McQuay, M.Q., Lacas, F., Rolon, J.C., Darabiha, N., and Candel, S., 2001, "Systematic measurements of OH chemiluminescence for fuel-lean, high-pressure, premixed, laminar flames," Fuel, **80**, pp. 67-74.

[23] Ayoola, B.O., Balachandran, R., Frank, J.H., Mastorakos, E., and Kaminski, C.F., 2006, "Spatially resolved heat release rate measurements in turbulent premixed flames," Combust. Flame, **144**, pp. 1-16.

[24] Polifke, W., Poncet, A., Paschereit, C.O., and Dobbeling, K., 2001, "Reconstruction of acoustic transfer matrices by instationary computational fluid dynamics." J. Sound Vib., **245**, pp. 483-510.

[25] Kato, S., Fujimori, T., Dowling, A.P., and Kobayashi, H., 2005, "Effect of heat release distribution on combustion oscillation," Proc. Combust. Instit., **30**, pp. 1799-1806.

[26] Kang, D.M., Culick, F.E.C., and Ratner, A., 2007, "Combustion dynamics of a low-swirl combustor," Combust. Flame, **151**, pp. 412-425.
[27] Sattelmayer, T., 2003, "Influence of the combustor aerodynamics on combustion instabilities from equivalence ratio fluctuations," J. Eng. Gas Turb. Power, **125**. pp. 11-19.
[28] Noiray, N., Durox, D., Schuller, T., and Candel, S., 2008, "A unified framework for nonlinear combustion instability analysis based on the flame describing function," J. Fluid Mech., doi: 10.1017/S0022112008003613.
[29] Truffin, K. and Poinsot, T., 2005, "Comparison and extension of methods for acoustic identification of burners," Combust. Flame, **142**, pp. 388-400.
[30] Kim, D., Lee, J.G., Quay, B.D., and Santavicca, D.A., 2008, "Effect of flame structure on the flame transfer function in a premixed gas turbine combustor," ASME Turbo Expo 2008, Berlin, Germany, June 9-13.
[31] Bellows, B.D., Bobba, M.K., Forte, A., Seitzman, J.M., and Lieuwen, T., 2007, "Flame transfer function saturation mechanisms in a swirl-stabilized combustor," Proc. Combust. Instit., **31**, pp. 3181-3188.
[32] Durox, D., Baillot, F., Searby, G., and Boyer, L., 1997, "On the shape of flames under strong acoustic forcing: a mean flow controlled by an oscillating flow," J. Fluid Mech. **350**, pp. 295-310.
[33] Dowling, A.P., 1997, "Nonlinear self-excited oscillations of a ducted flame," J. Fluid Mech., **346**, pp. 271-290.
[34] Peracchio, A.A. and Proscia, W.M., 1999, "Nonlinear heat release/acoustic model for thermo-acoustic instability in lean premixed combustors," J. Eng. Gas Turb. Power, **121**. pp. 415-421.
[35] Kim, K.T., Lee, J. G., Lee, H.J., Quay, B., and Santavicca, D., "Characterization of forced flame response of swirl-stabilized turbulent premixed flame," GT2009-60031, submitted.
[36] Schuller, T., Durox, D., and Candel, S., 2003, "Self-induced combustion oscillations of laminar premixed flames stabilized on annular burners," Combust. Flame, **135**, pp. 525-537.
[37] Schuller, T., Durox, D., and Candel, S., 2003, "A unified model for the prediction of laminar flame transfer functions: comparisons between conical and V-flame dynamics," Combust. Flame, **134**, pp. 21-34.
[38] Garcia, M.C., Mastorakos, E., and Dowling, A.P., 2009, "Investigations on the self-excited oscillations in a kerosene spray flame," Combust. Flame, **156**, pp. 374-384.
[39] Lieuwen, T., McDonell, V., Santavicca, D., and Sattelmayer, T., 2008, "Burner development and operability issues associated with steady flowing syngas fired combustors," Combust. Sci. and Tech., **180**, pp. 1167-1190.
[40] Buchner, H., Hirsch, C., and Leuckel, W., 1993, "Experimental investigation on the dynamics of pulsated premixed axial jet flames," Combust. Sci. and Tech., **94**, 219-228.